TIBAGS: Tropospheric Iodine Monoxide and Its Coupling to Biospheric and Atmospheric Variables—a Global Satellite Study

Anja Schönhardt, Andreas Richter and John P. Burrows

Abstract In the framework of the TIBAGS project, spatial and temporal variations of iodine monoxide, IO, in the Earth's atmosphere were analysed, and relations between IO and further variables of the biosphere and atmosphere were investigated. The abundances and variations of IO are not well known on a global scale, partly because IO amounts are comparably low. However, due to strong reactivity, also small amounts of IO may have a substantial impact on tropospheric composition. In the present study, satellite data from the SCIAMACHY (Scanning Imaging Absorption spectrometer for Atmospheric CHartographY) sensor on board the ENVISAT satellite is used and a more global view on the subject is obtained. IO amounts are retrieved from measurements of scattered sunlight by using an absorption spectroscopy technique. Two consistent IO data sets are retrieved, one based on near real-time data (2004–2011) and one based on reprocessed consolidated data (2003–2010). Largest amounts of IO are found in the Polar Regions of Antarctica, for example in the Weddell Sea area in spring time. In addition, enhanced IO amounts are detected above some but not all biologically active ocean areas which show high Chlorophyll-a (Chl-a) signals. Correlations between IO and diatom distributions are in some areas stronger than between IO and Chl-a in general, indicating the importance of the specific phytoplankton species present in the ocean water.

1   Background Information

The focus of the TIBAGS project is set on the trace gas iodine monoxide in the atmosphere. Iodine compounds are relevant for tropospheric composition for several reasons. Iodine radicals react with ozone, whereby iodine monoxide, IO, is formed and tropospheric ozone is destroyed. This also affects levels and lifetimes of

A. Schönhardt (✉) · A. Richter · J.P. Burrows
Institute of Environmental Physics, University of Bremen, Otto-Hahn-AHee 1, 28359 Bremen, Germany
e-mail: schoenhardt@iup.physik.uni-bremen.de

other tropospheric species. In addition, IO may lead to the formation of fine atmospheric particles which influence the radiation budget. IO is hence an indicator of active iodine photochemistry, and iodine chemistry is considered to be relevant for understanding tropospheric composition, especially in the marine boundary layer and Polar Regions (e.g. [6, 22], and references therein). Precursors of IO include molecular iodine, I_2, as well as halocarbons. These may be emitted, e.g. by algae and phytoplankton ([15], and references therein), or via inorganic pathways from the ocean [7].

Several field studies have investigated these precursors as well as atmospheric levels of IO. However, all field studies are necessarily restricted in time and space, and the spatial and temporal distributions of atmospheric iodine are only partly known. Satellite measurements are an additional and valuable source of information as they yield near global observations over time scales of many years.

In the framework of the TIBAGS project, abundances of IO are retrieved from space on a nearly global scale. The retrieval of IO from the Scanning Imaging Absorption spectroMeter for Atmospheric CHartographY (SCIAMACHY) has initially been demonstrated by Schönhardt et al. [24]. Based on near real-time data, now the time series covers the years 2004–2011. Comparisons between the amounts and distributions of IO with selected parameters of the atmosphere and biosphere shall improve our understanding of source regions and links to other processes. The studied parameters include atmospheric trace gases such as bromine monoxide, BrO, and the short-lived organic compounds formaldehyde, HCHO, and glyoxal, CHOCHO, as well as compounds dissolved in the ocean waters such as Chlorophyll-a and individual phytoplankton species.

Focus areas of the TIBAGS project are the Polar Regions, especially Antarctica, as well as the world's ocean areas. An overview of IO above Antarctica is shown in Fig. 1. The Southern Hemispheric map depicts the average IO vertical column

Fig. 1 Average IO vertical column amounts for eight years (2004–2011) above the Antarctic region
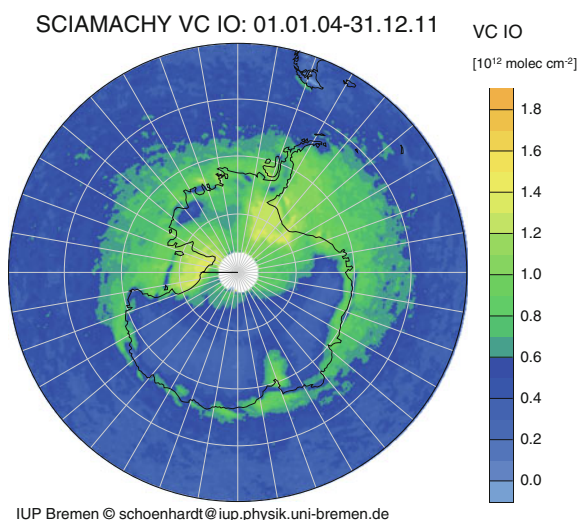
amount for the eight years from 2004 to 2011. IO amounts are enhanced above the sea ice region, above the shelf ice, along the coast lines, as well as above parts of the continent. Details on the IO retrieval and the resulting observations are described in the following sections.

2 The Satellite Sensor

Column amounts of IO may be retrieved by using absorption spectroscopy. The well-established and widely used method of differential optical absorption spectroscopy (DOAS) [16, 17] was applied in the present study to detect IO amounts in the radiances recorded by the SCIAMACHY sensor on board the European Space Agency's (ESA's) Environmental Satellite ENVISAT. SCIAMACHY is a spectrometer measuring in the ultraviolet (UV), visible and infrared (IR) wavelength regions, in three different geometries: nadir, limb and occultation [3, 5, 11, 12]. In the present study, nadir measurements in the visible were used.

3 Data Analysis

The DOAS retrieval initially yields slant column amounts of IO, which describe the amount of IO integrated along the slant light path. The slant columns are the result of a least-squares optimization routine based on the Lambert–Beer law. An actual radiance measurement I is compared to a background measurement I_0, which in the present case is an Earthshine radiance chosen from a background region. The difference between the two measurements is caused by several atmospheric effects, including absorption, scattering and reflection, of the electromagnetic radiation. Absorption by trace gases in the atmosphere is one important contribution. In the DOAS method, only those spectral effects, which quickly vary with wavelength (high-pass filter), are further analysed. Low-frequency effects are effectively filtered out by the subtraction of a polynomial, a quadratic polynomial in the present case.

The applied DOAS retrieval for IO uses the wavelength window between 416 and 430 nm. The IO absorption cross-section measured by Gómez Martín et al. [10] is applied to identify the IO absorption bands in the measurements. Additional trace gases taken into account are O_3 and NO_2. In addition, the Ring effect is taken into account, an effect that is caused by inelastic scattering on molecules in the Earth's atmosphere and leads to an infilling of absorption lines, especially the solar Fraunhofer lines. The Ring effect is calculated separately by radiative transfer (RTF) calculations, and an effective Ring spectrum is fitted as a pseudo-absorber cross-section in the same manner as the trace gases. A linear intensity offset is also taken into account.

4   Considerations on the Air Mass Factor

As the slant column is intrinsically dependent on the respective light paths which the radiation has taken through the absorber layer(s), this light path needs to be estimated when the slant columns are to be converted into the more comprehensible values of vertical columns. The vertical column is the amount of the absorber per ground area integrated vertically through the atmosphere and usually given in molecules per cm^2 (molec/cm^2). The light path taken by the radiation going from the sun through the atmosphere and into the satellite sensor is computed by RTF calculations.

In the present study, the RTF code SCIATRAN is applied [20] to calculate the so-called air mass factor (AMF) which is the light path length through the absorber layers relative to a single vertical transmission. Hence, the vertical column VC_i of trace gas i is given by the ratio of the slant column SC_i to the AMF a.

$$VC_i = \frac{SC_i}{a(\lambda, p)}$$

The calculated AMF a depends on the wavelength λ and on a parameter set p including, e.g. the surface reflectance, solar zenith angle and the absorber profile. The parameters used in the RTF calculation need to be adapted to the respective measurement scenario.

By considering the variation of AMF with the solar zenith angle, SZA, the dependency of the slant column value on the SZA is effectively eliminated in the vertical column value. For satellite geometry in nadir observation, typical variations of AMF with changing SZA are shown in Fig. 2.

The left graph is computed for a Polar scenario with snow/ice cover and corresponding albedo of 0.9, and SZA variation from 30 to 84°. The standard IO
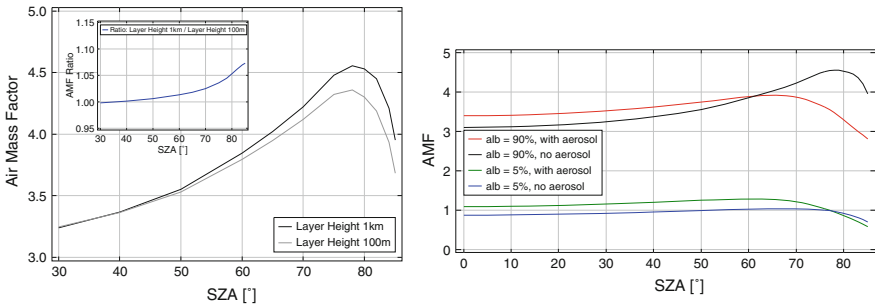

Fig. 2 *Left* AMF for IO at 90 % albedo calculated for different mixing layer heights, for 1 km shown in *black* and for 100 m shown in *grey*. The *inset* shows the ratio of the two curves, maximum deviation at large SZA does not exceed about 7 %. *Right* AMF for different scenarios, testing the influence of aerosols on the IO AMF for a bright (90 %) albedo scene (*red* and *black* curves) and a dark (5 %) albedo case (*green* and *blue* curves)

retrieval only uses measurements up to 84° SZA, as the signal-to-noise ratio (SNR) strongly decreases for larger angles. The left figure compares the AMF for two different profiles, both box profiles of constant mixing ratios, one going from the ground up to 1 km (black), the other from ground to 100 m (grey). The actual IO profile is not well known. Recent observations report on IO in the free troposphere [8, 18], but IO is mostly found in the boundary layer (e.g., [6, 21]).

For the results in Fig. 2, a pure Rayleigh atmosphere is considered, i.e. without scattering on aerosols. For Antarctica, this is a valid first assumption. The largest difference of 7 % between the two settings is found for large SZA. As the influence of the mixing layer height on the AMF is comparatively small for this high albedo scene, the choice of the layer height does not influence the derived IO vertical column amount much. The results from the black curve with 1 km mixing layer height are typically used for the calculation of the vertical IO columns in Polar studies such as the Antarctic map in Fig. 1.

Aerosols are frequently present in other scenes and may strongly influence the AMF as the light path is influenced by additional scattering processes on the aerosol particles. Whether the AMF increases or decreases with aerosol load depends on the relative vertical position of the aerosol and absorber layers as well as on the aerosol type. The right graph of Fig. 2 presents the aerosol influence on the AMF value. As an example case for ocean scenarios, the aerosol type considered here is maritime aerosol with a visibility of 10 km. The aerosol is mixed with the IO layer and is partly situated above the IO. The calculated AMF results are again plotted versus SZA, where the cases for 90 % albedo are shown in red and black (with and without aerosols) for comparison, and the cases for 5 % albedo typical for water surfaces are shown in green and blue. For small SZA, aerosols enhance the sensitivity towards IO detection, i.e. lead to an increase of the AMF. For the bright case of 90 % albedo, the enhancement lies around 10 %, while for the dark scene, aerosols enhance the sensitivity by around 25 %. At larger SZA (>62° for 90 % albedo, and >77° for 5 % albedo), aerosols lead to a decrease of the AMF. Only for the 90 % case at low sun (large SZA) a difference larger than 25 % is found with lower sensitivity in the presence of aerosols. For smaller SZA, therefore, not considering aerosol influence on the AMF may lead to a limited overestimation of IO vertical columns while for larger SZA, some underestimation may occur.

In the details, therefore, the IO amount is dependent on the aerosol load, but for moderate aerosol amounts, the influence does not dominate over regional or temporal changes. The IO overview maps presented in the next sections are computed for aerosol-free scenarios.

5 Detection Limit and Averaging

Considering slant column amounts, the IO detection limit for a single SCIAMACHY measurement lies at 7×10^{12} molec/cm^2. The vertical column detection limit depends on the AMF. Above snow and ice, the detection limit lies

around 1.7×10^{12} molec/cm^2. As the IO amounts are often not much larger than the detection limit, temporal and/or spatial averaging is necessary to improve SNR and thus data quality. In addition, absolute IO amounts need to be treated with caution. IO maps are typically generated as averages over time spans of several months. This way, the statistical error on the measurements is reduced. In order to resolve smaller scale temporal variations, single calendar months of subsequent years are averaged. Using this strategy, a time series of IO maps through different seasons may be generated (cf. Sect. 6).

6 Observations Above Antarctica

Using SCIAMACHY satellite data, both IO and BrO are retrieved for many years and compared for the same time periods above the Southern Hemisphere. Also based on satellite observations, the regions of IO enhancement are compared to the sea ice cover in the respective time periods.

6.1 Spatial and Temporal Variations of IO Vertical Columns

The temporal averaging period in order to obtain a SNR of sufficient quality for the IO vertical column product depends on several aspects such as the time of year, the location on the Earth and the surface conditions. Usually, a suitable averaging period for IO data is a few months.

In order to resolve temporal variations in the IO amounts not only on a seasonal basis but on a smaller time scale, IO columns of single calendar months are averaged over subsequent years. In this way, monthly variations which reoccur every year can be resolved. This procedure is suitable owing to the fact that many features in the spatial pattern of IO are repeated annually. As a result, monthly maps, each averaged over eight years from 2004 to 2011, are produced. They are used for comparison with BrO columns and other parameters. The temporal evolution of IO enhancements above the Antarctic regions is thus observed. In Schönhardt et al. [23] maps for the time period 2004–2009 have been published. Figure 3 shows the time series of IO from October (Antarctic spring time) through summer to March (Antarctic autumn).

For direct comparison, the same time series is plotted for BrO vertical columns in Fig. 5 in Sect. 6.2 below.

IO amounts in September are rather scattered due to low light levels resulting in lower signal at the satellite. Some locally enhanced IO amounts along the coast west of the Antarctic Peninsula are detected and some scattered amounts above the ice shelves. In October, enhanced IO vertical columns of up to about 1.6×10^{12} molec/cm^2 are spread over wide parts of the shelf ice areas, especially
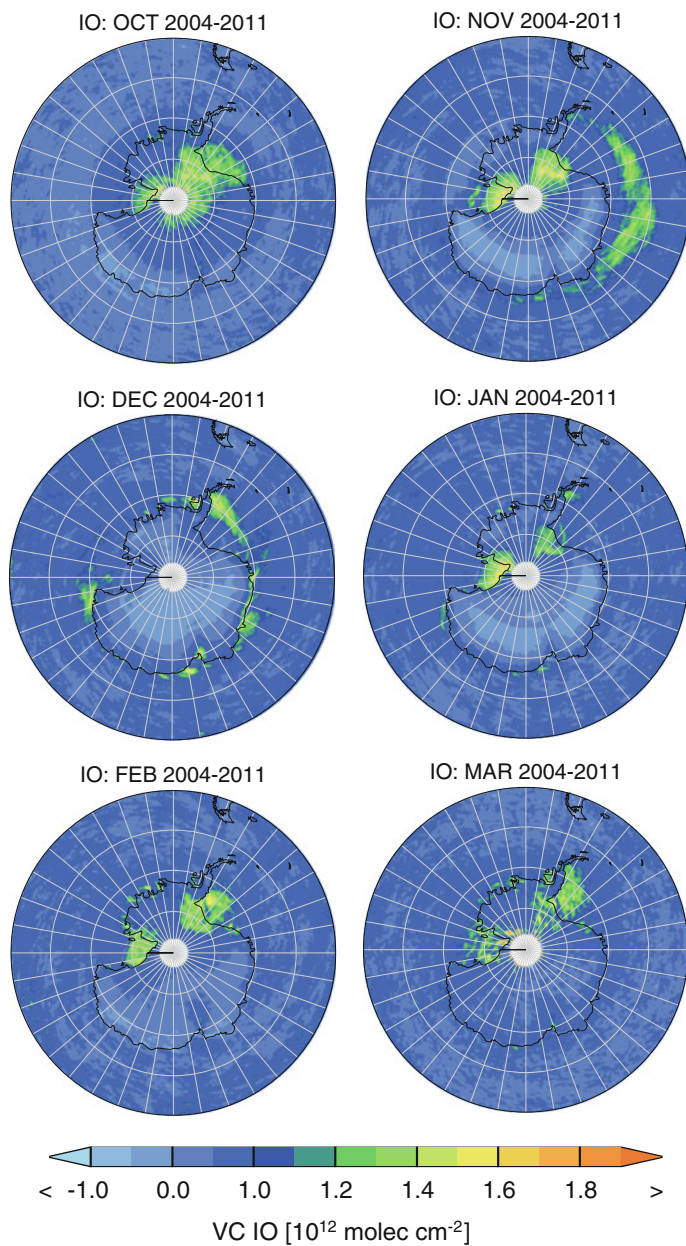
Fig. 3 Monthly averages of IO vertical columns above the Antarctic continent for eight years (2004–2011). The AMF applied here assumes a ground reflectance of 90 % suitable for clean snow and ice

the Weddell Sea and the Ross Sea areas, in coastal locations and the continent. Between October and November then a distinct feature of IO enhancement evolves at some distance of the coast, and has fully developed into a circular region of IO amounts above the sea ice in the November average. The circular enhancement retreats somewhat in December and moves closer to higher latitudes, and IO is still visible along the coasts on some sea ice patches. Later in autumn (January/February), IO is mostly found on the shelf ice areas. In parts, the areas of IO occurrence overlap and agree with the sea ice cover.

The main spatial features are repeated from year to year. This is demonstrated by Fig. 4 showing Antarctic monthly means of IO observations for one year (top row), six years (middle row, the time period used in Schönhardt et al. [23]) and the full eight years of the IO near real-time product (bottom row). A longer averaging period reduces noise effects and emphasizes the main features of IO enhancement. For the comparison in Fig. 4, the calendar months November (left column), December (middle column) and January (right column) have been chosen, as the IO spatial pattern changes noticeably during this time of year with enhanced IO amounts above the ring-shaped sea ice around Antarctica in November, and reducing amounts and spatial extent towards January.

Clearly, local values may be larger when using shorter averaging periods. It is remarkable, however, that spatial patterns and IO amounts are conserved rather clearly when averaging over several years. Some persistence in the seasonal variation of IO is the reason for this behaviour.

6.2   Comparison of IO and BrO Distributions

Bromine monoxide, BrO, is a molecule that is in principle similar to IO. However, the atmospheric relevance as well as sources and sinks may be quite different. In the Polar Regions, BrO is regularly generated by a mechanism called the bromine explosion (cf., e.g. [25], and references therein). During these events that begin shortly after Polar sunrise in early spring time, atmospheric BrO increases rapidly and is present above large areas. The release mechanism is an inorganic process. The relevant and necessary conditions for the bromine explosion to take place are a matter of continuing research.

In order to investigate the relations between IO and BrO distributions, satellite observations of the two species are compared. BrO vertical columns are retrieved from SCIAMACHY observations in the UV wavelength range [19, 30]. Taking into account the stratospheric amounts of BrO, a stratospheric AMF has been applied [19]. More details on AMF considerations for BrO observations can be found in studies by Begoin et al. [2] and Theys et al. [27]. The BrO data were averaged for the same periods and the same region as for IO and are shown in Fig. 5.

The BrO distributions show some clear differences towards the IO observations, but also some general similarities. One similarity lies in the fact that both, IO and
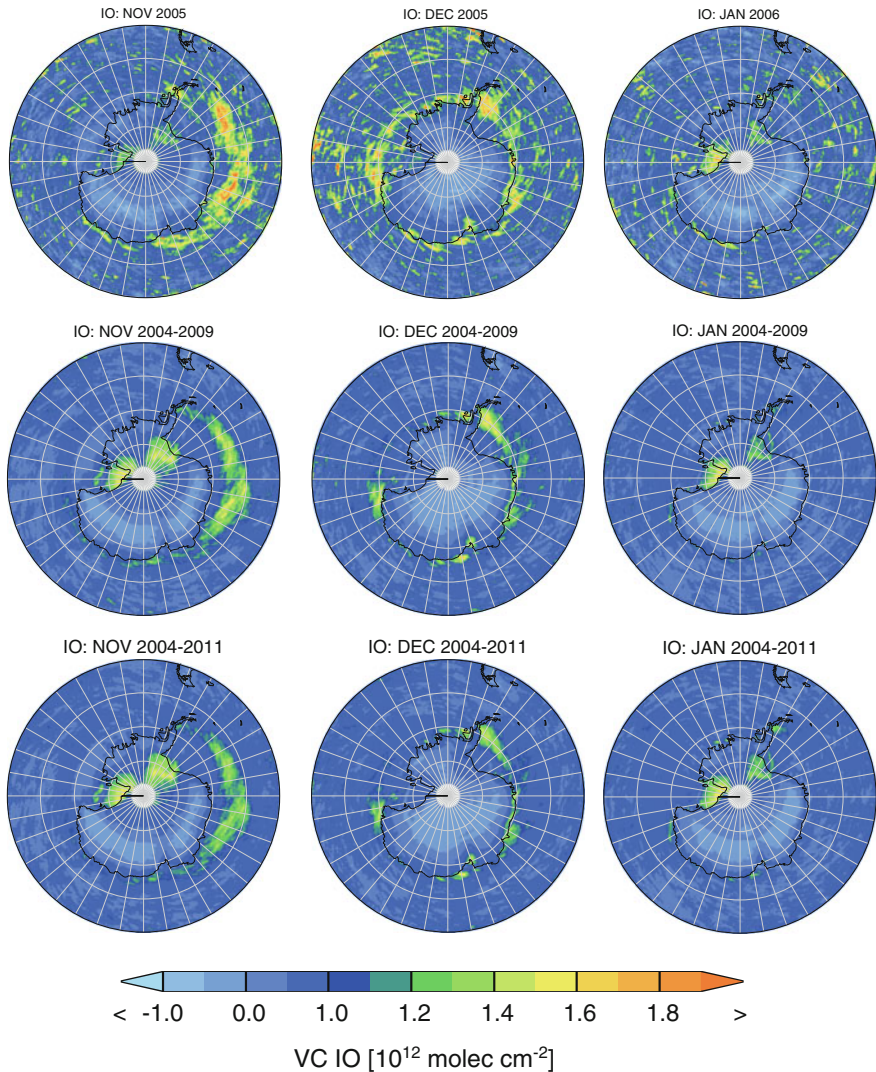
Fig. 4 Comparison of IO vertical columns over Antarctica for an averaging period of one year (*top row*), six years (*middle row*, as used in Schönhardt et al. [23]) and eight years (*bottom row*). Main patterns and regional enhancements of IO reappear from year to year

BrO amounts, are enhanced above the Antarctic region in spring time. The details of the spatial and temporal distributions however, are quite different. BrO is mostly present above the sea ice around the continent, and enhancement starts with Polar sunrise in August (not shown), and is fully developed in September. Through the summer months, BrO amounts decrease and mostly vanish in autumn, except for
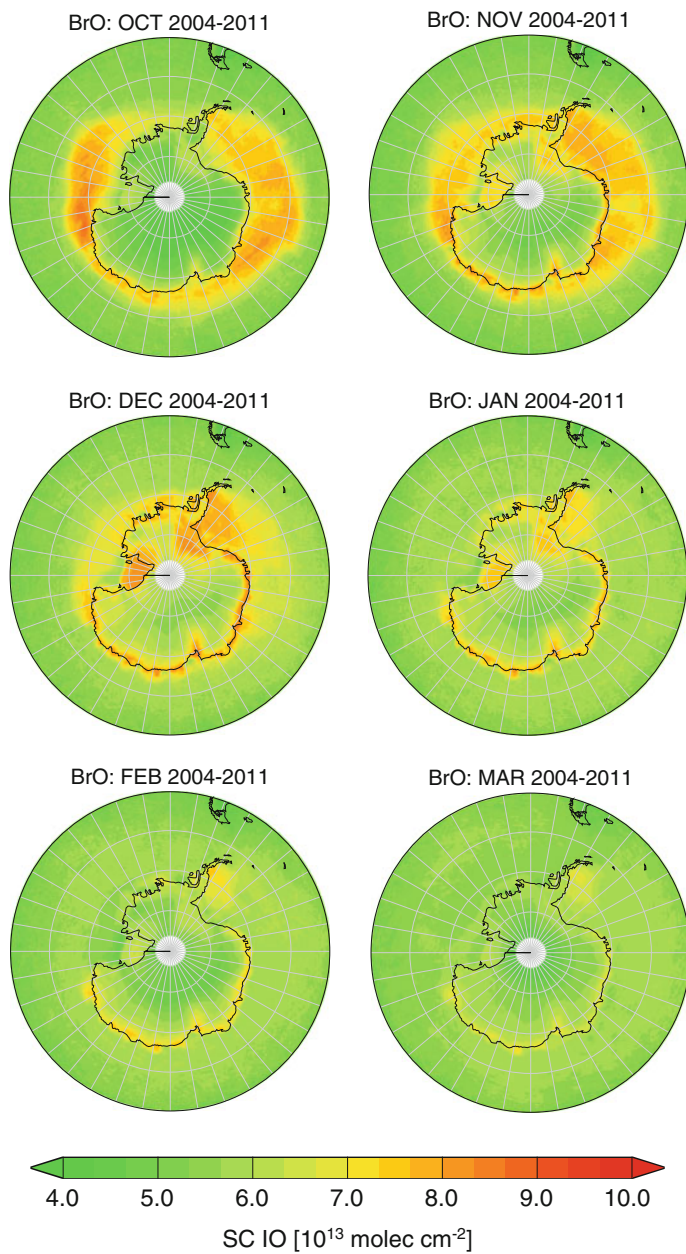
BrO: OCT 2004-2011   BrO: NOV 2004-2011

BrO: DEC 2004-2011   BrO: JAN 2004-2011

BrO: FEB 2004-2011   BrO: MAR 2004-2011

4.0   5.0   6.0   7.0   8.0   9.0   10.0

SC IO [10^{13} molec cm^{-2}]

Fig. 5 BrO vertical column averages above the Antarctic region for the same averaging periods as for IO in Fig. 3

enhancements along the coast lines and above the ice shelves (there especially in December and January).

Resulting from the differences between the IO and BrO spatial and temporal distributions, it can be concluded that at least some individual release pathways exist for iodine and bromine species in the South Polar Region. Although both, IO and BrO, occur in Antarctic Spring time, IO is present above the sea ice for a comparably shorter time period concentrated more towards later spring, while BrO is already present on the sea ice prominently from early spring onwards.

6.3   Relation of the Halogen Oxides to Sea Ice Cover

Both halogen oxides, IO and BrO, show enhancements above the sea ice covered area around the Antarctic continent. Comparisons with sea ice cover data have been performed using ice concentration data from the AMSR-E instrument [13, 26]. AMSR-E is the Advanced Microwave Scanning Radiometer for EOS, a passive microwave radiometer on board the NASA AQUA satellite belonging to the Earth Observing System (EOS). The ice concentration data is provided by ZMAW (Centre for Marine and Atmospheric Sciences) in Hamburg, Germany, and can be downloaded from the Integrated Climate Data Center, KlimaCampus, at the University of Hamburg (ICDC, http://icdc.zmaw.de/seaiceconcentration_asi_amsre. html?&L=1). The ice concentration is defined as the percentage of the representative AMSR-E satellite pixel covered by sea ice.

Figure 6 (right) shows the monthly ice concentration for November averaged over six years from 2004 to 2009, together with the IO map (left) for the same time period. The close spatial correlation of sea ice area with BrO enhancements
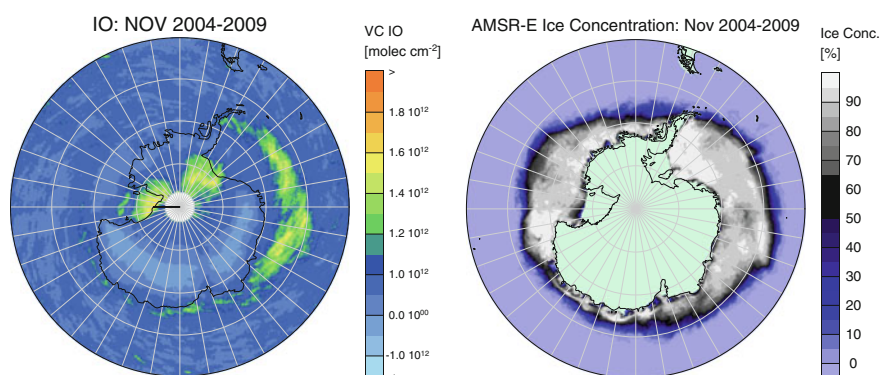

Fig. 6 IO vertical columns (*left*) from SCIAMACHY observations and ice concentration (*right*) derived from AMSR-E data in November above the Southern Polar Region averaged over six years from 2004 to 2009. The ice map is based on daily data provided by the Integrated Climate Data Center, Hamburg (http://icdc.zmaw.de)

(cf. Fig. 5) is apparent. In addition, the curved region of enhanced IO in November is located above still present sea ice. In November, the density of the sea ice is reduced in some areas, as visible in Fig. 6 by darker grey patches within the sea ice area. The ice sheets start to break up and retreat in spring time. When the sea ice becomes more porous, and more open leads and polynyas develop, the water gets into contact with the atmosphere above. As iodine compounds are presumably emitted by biological species such as phytoplankton or ice algae, which prefer the habitat underneath the sea ice sheets, iodine input to the atmosphere may be facilitated as soon as the ice sheets break up. Convection above open water areas further supports the insertion of gaseous species, as the water is warm compared to the spring time Antarctic boundary layer air. These considerations form a possible explanation for the temporal behaviour of the observed IO occurrence in late spring. As further evidence of a connection to a biological source, Chlorophyll-a data have been consulted. This is discussed in Sect. 7.

In addition to providing a habitat for biological species, the sea ice cover also changes the radiation conditions in the respective areas. This has two consequences. On one hand, the stronger light reflection improves the visibility of IO above ice covered regions. On the other hand, the photochemical situation is different above and next to the ice. While the first aspect enhances the observed IO amounts above sea ice, the second aspect can influence in both directions, as iodine precursors as well as the IO amount itself are altered by changing light conditions. In any case, the Antarctic ice region is an especially interesting area for iodine research.

In a study by Atkinson et al. [1], the Weddell Sea area has been selected as focus area for iodine measurements in and above the sea ice and the ocean. The field study includes measurements in the water, ice and atmosphere, and the results emphasize that the Weddell Sea area is rich in iodine chemistry. Atmospheric iodine chemistry, however, is not yet well enough understood to make full atmospheric modelling possible. Not all observed data may be reproduced by model calculations. Some iodine source terms might still be unknown.

7 Relations Between IO and Biospheric Parameters

Previous studies have demonstrated that iodine compounds are emitted by biological species such as microalgae and macroalgae. Several chemical compounds are thereby emitted by various organisms in different speciations and different amounts [9, 28]. Satellite IO observations are compared to Chlorophyll-a (Chl–a) concentrations in the oceans, an indicator of active biology. For this comparison, IO data from a reprocessed data set for 2003–2010 is used. The data set is fully consistent with the near real-time data set from 2004 to 2011, but includes a more complete time series during the initial year 2003. For the investigation of Chl-a concentrations, the ESA merged GlobColour product is used. This product is based on the three instruments SeaWiFS (Sea-viewing Wide Field-of-view Sensor), MERIS (Medium Resolution Imaging Spectrometer) and MODIS (Moderate

Resolution Imaging Spectroradiometer). Information and data are available from the website http://www.globcolour.info.

7.1 Comparison Between IO and Chlorophyll-a Above Antarctica

The oceans surrounding the Antarctic continent are a region of strong biological activity. Following the detection of IO within the sea ice zone above the biology-rich waters, the first interesting comparison is that of IO and Chl-a around Antarctica. Long-term averages over many years are compiled and presented in Fig. 7 for IO (left) and Chl-a concentrations (right). IO vertical columns are computed here with an AMF that assumes a surface albedo of 5 %, appropriate for oceans in the visible spectral range. A spatial mask is applied to the IO data, showing the results only for regions, where Chl-a data is also available. The Chl-a data can only be derived from above-satellite ground pixels which are entirely free of ice, otherwise the signal from the ice covered part of the field-of-view would dominate the measured signal. This way, also the IO data is plotted only above regions which are at least for some part of the year free of ice. As the low albedo is applied, IO amounts in this map differ from the ones above. Some overestimation of the absolute IO amount may occur when applying the low albedo scenario.

Two main features can be derived from Fig. 7. First of all, the Antarctic proves to be an area rich in biological productivity, demonstrated by fairly large Chl-a concentrations all around the Antarctic continent with local maxima in the Weddell Sea, the Ross Sea and just off the coast over long distances as well as the area
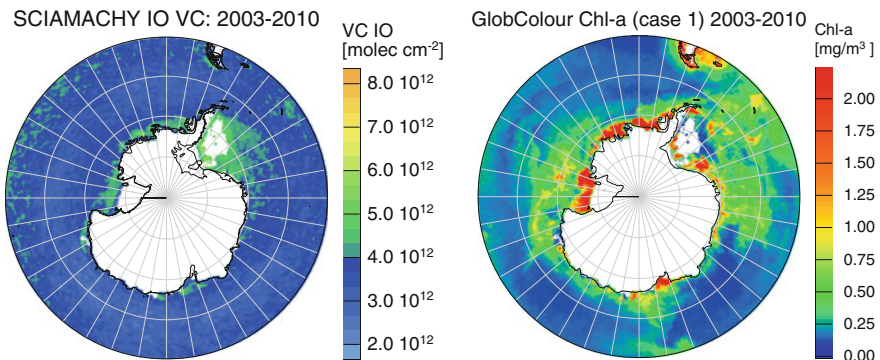

Fig. 7 Antarctic maps of IO vertical columns in the atmosphere (*left*) and Chlorophyll-a concentrations in the ocean (*right*). For the IO data, conversion to vertical columns assumes an albedo of 5 % suitable for observations above water bodies, and data is masked by the area, where Chl–a data is available, i.e. data is only shown above regions which are free of ice at least in parts of the year

offshore of the Amery ice shelf. The second striking observation is the spatial overlap of enhanced values of IO with many of these Chl-a rich locations. Especially the Weddell Sea and the waters of the Ross Sea offshore of the Ross ice shelf show both, enhanced IO and enhanced Chl-a, in similar spatial patterns. Naturally, a correlation does not represent causality. However, from this comparison, a relation between biological production and the release of iodine precursors seems probable.

7.2 Comparison Between IO and Chlorophyll-a Above Ocean Areas

In contrast to the Antarctic analysis, spatial correlation between IO and Chl-a is not a general feature elsewhere. Other regions on the globe do not show such a clear spatial relation. Especially, regions with strong biological productivity can be found where no significant IO signal is detected.

For biological productivity, the ocean upwelling regions are important. Here, colder deep water masses rise to the surface and are often rich in nutrients and organically produced gaseous compounds may enter the atmosphere. Figure 8 compares atmospheric IO amounts from SCIAMACHY with oceanic Chl-a
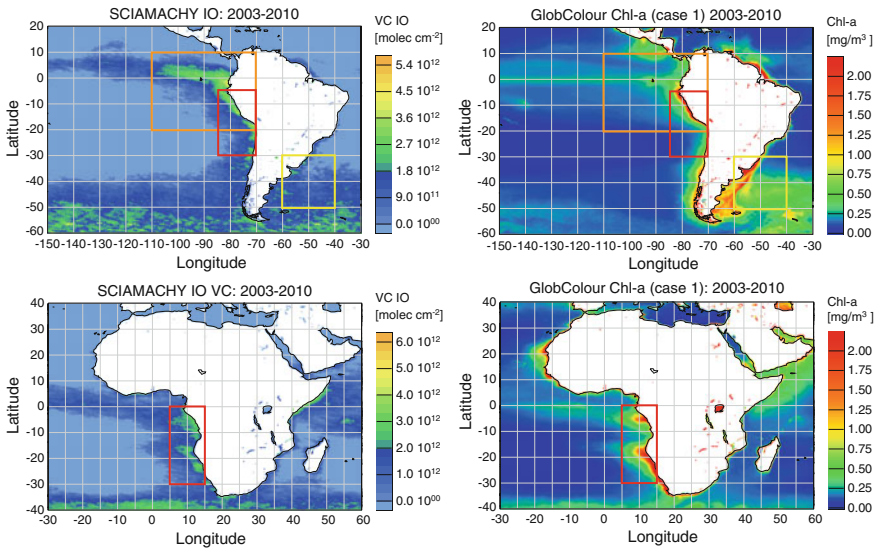

Fig. 8 Comparison of eight year averages (2003–2010) of atmospheric IO (*left*) and oceanic Chl–a concentrations (*right*). The areas marked by coloured boxes are used for the computation of spatial correlation coefficients

concentrations from the GlobColour project, both for an eight year average from 2003 to 2010. The maps in the top show the Eastern Pacific and Southwest Atlantic around South America, and the bottom maps focus on the waters around Africa. Field studies have also reported on elevated IO amounts above the Eastern Pacific [8, 14, 29]. Along the West coast of South America, a large upwelling region is situated where the Humboldt current from Antarctica surfaces. As seen in the enhanced Chl-a data, off the coasts of Peru and Chile, biological activity is present. Enhanced Chl-a amounts are also seen further into the Pacific towards the Galápagos Islands.

Above the Peru and Northern Chile upwelling area, Chl-a enhancements coincide with enhanced IO abundances, which also spread further into the ocean towards the Galápagos Islands. Around the South tip of Chile and Argentina, where Chl-a is large especially on the East coast, IO amounts are smaller and the relation between the two compounds is less prominent. North of Brazil, around the Amazon estuary, the Chl-a amounts are large, and IO amounts are also detected, however, much less strongly as compared to the Eastern Pacific. For the coloured boxes in Fig. 8 (top), example correlation coefficients for the spatial correlations are determined to be $r = 0.29$ and 0.27 for the yellow and orange areas, respectively, and somewhat larger at $r = 0.43$ for the red box, each with an uncertainty around 0.02. These coefficients are not overly large, but significantly positive, and the red box close to the coast reveals the strongest correlation of these three areas.

Around the African continent the diverse relation can be seen even better. Figure 8 (bottom) shows that Chl-a is enhanced especially above the Mauritanian upwelling region (off the African Northwest coast) and above a two parted area off the African Southwest coast, partly coinciding with the Benguela current. In the Southwest, the spatial patterns of IO and Chl-a are very similar, while in contrast, no significantly enhanced IO is found above the Mauritanian upwelling in the North. For the Southwest region marked by a red box, the spatial correlation lies at $r = 0.50$.

The Chl-a and IO spatial patterns are also similar, e.g. towards the open ocean at the Southern limit of the displayed map as well as at the West coast of Somalia. Clear differences appear along the coasts of the Arabian Peninsula where no enhanced IO is detected above areas where Chl-a is present.

All in all, an ambiguous picture is received from the analysis of Fig. 8. Enhancements in IO and Chl-a concentration coincide for some areas, while other locations do not exhibit a spatial relation between the two variables, i.e. Chl-a concentrations are high while no large IO is found. Possibly, the phytoplankton types as well as surface and atmospheric conditions or other than direct biological source pathways play a role for the emissions of iodine compounds.

7.3 Comparison Between IO, Chlorophyll-a and Diatoms for Southeast Asia

Following from the ambiguous picture discussed in the previous section, investigations of individual phytoplankton types are of interest. Using the PhytoDOAS method [4], a few different phytoplankton species may be distinguished. From the absorption spectrum characteristic for each different organism, the PhytoDOAS method retrieves an equivalent Chlorophyll-a concentration indicative of the amount of phytoplankton present in the light absorbing upper ocean layers. In the context of iodine release, the distributions of diatoms are specifically interesting and have therefore been investigated for some selected regions. Diatom maps display the equivalent Chl-a amount, which should be proportional to the amount of diatom organisms in the upper ocean layers. The absolute diatom amount still depends somewhat on the unknown vertical phytoplankton profile.

Figure 9 shows the comparison of IO abundances (top), total Chl-a concentration (bottom left) and Chl-a from diatoms (bottom right) in the oceans of Southeast Asia. This region is of specific importance for the exchange between the stratosphere and the troposphere because of strong convective transport. Therefore, this area is the
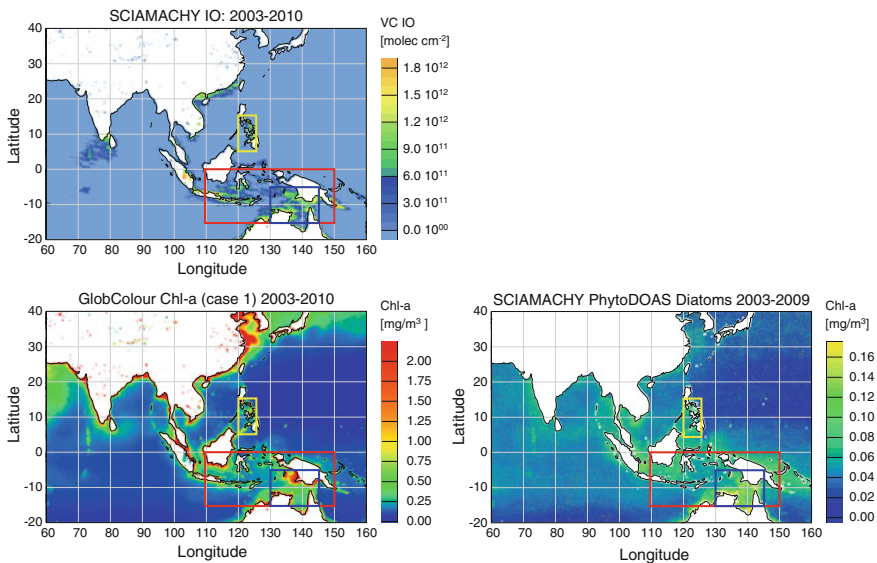

Fig. 9 Comparison between long-term averages of atmospheric IO (*top*) with total Chl-a (*bottom left*) and Chl-a from diatoms (*bottom right*) in the oceans of Southeast Asia. Marked areas are used for example calculations of spatial correlation coefficients. In several locations, a spatial relation between IO and diatoms, as well as between IO and total Chl-a is observed, while other areas such as the East China Sea are rich in Chl-a with no diatoms and no IO. Diatom data are courtesy of Astrid Bracher, AWI Bremerhaven and Tilman Dinter, University of Bremen, in the framework of HGF project Phytooptics and EU project SHIVA

central research area of the SHIVA project (Stratospheric Ozone—Halogen Impacts in a Varying Atmosphere). Data is averaged over the years 2003–2010, for diatoms from 2003 to 2009 as data of the year 2010 was not available.

Several locations show enhanced IO, where Chl-a and diatoms are present in the water, especially at some coast lines, e.g. of Southern China, and between some islands, such as between the Philippines, between New Guinea and Australia, and further west in the sea gate between Sri Lanka and India. In most of these locations, the Chl-a content in the water is large, and diatoms are detected, except for the coast of Southern China, with large Chl-a but little diatom detections.

On the other hand, there is strong Chl-a occurrence in the Yellow Sea and East China Sea, but no IO is detected there and diatoms are not prominent there either.

Further to the qualitative comparison of the regional maps, some spatial correlation coefficients have been computed. For example, the areas between the islands as marked by three coloured boxes in Fig. 9 have been analysed. For IO and Chl-a, the correlation coefficients are $r = 0.33$, 0.31 and 0.38 for the yellow, red and blue areas, respectively. For IO and diatoms, the correlation coefficients are larger with $r = 0.48$, 0.47 and 0.62, respectively.

These results and observations are a further indication that there is no general one-to-one relationship between iodine compounds and all Chl-a producing biological species. If iodine species are biogenically produced, some differentiation amongst the emitting phytoplankton species is taking place which is strong enough that it becomes noticeable in the satellite measurements. In the selected regions, IO abundances correlate much better with the diatom distributions than with total Chl-a patterns, while the enhanced IO is not accompanied by strong diatom occurrence at the coast of South China. Consequently, although diatoms show a closer relation with IO in several locations than Chl-a, also diatoms are no safe indication for iodine emissions. Although the picture remains to some extent ambiguous, the spatial overview from satellite reveals many interesting regions with a spatial link between IO and the underlying biological situation.

8 Summary

The TIBAGS project has provided the opportunity to continue research on atmospheric iodine measured from space. Long-term data sets of IO observations from the SCIAMACHY instrument have been retrieved and investigated in order to increase our knowledge on spatial and temporal distributions and variations of atmospheric IO abundances. Largest amounts of IO have been detected in the Antarctic, and in the long-term data sets re-occurring IO maxima in the same regions each year have been found. Comparisons between IO and BrO above the South Polar Region show that besides the mutual appearance in Antarctic Spring, the spatial distribution as well as the temporal evolution differ in their details. Separate release pathways are most probably the reason for the differences.

In ocean areas around the South American and African continent, Chlorophyll-a concentrations in the ocean waters coincide with enhanced IO in several places but not in all. The spatial correlation between IO and Chl-a in some places suggests the importance of biological activity, while the missing one-to-one relationship indicates that other influencing factors are relevant for the release of iodine from the ocean. In the ocean areas of South-East Asia, correlations between IO and Chl-a as well as between IO and diatoms, a specific phytoplankton species known to emit iodine precursor substances, have been investigated. Spatial correlation coefficients between IO and diatom abundances are larger than between IO and total Chl-a, supporting the laboratory result that iodine release is to some extent dependent on the prevalent phytoplankton species. Closer investigations in ocean areas are needed to further improve our understanding on iodine release. Efforts should include field studies on local air composition and measurements of gaseous compounds as well as phytoplankton species in the ocean waters in addition to continuing long-term satellite observations.

References

1. Atkinson HM, Huang R-J, Chance R, Roscoe HK, Hughes C, Davison B, Schönhardt A, Mahajan AS, Saiz-Lopez A, Hoffmann T, Liss PS (2012) Iodine emissions from the sea ice of the Weddell Sea. Atmos Chem Phys 12:11229–11244. doi:10.5194/acp-12-11229-2012
2. Begoin M, Richter A, Weber M, Kaleschke L, Tian-Kunze X, Stohl A, Theys N, Burrows JP (2010) Satellite observations of long range transport of a large BrO plume in the Arctic. Atmos Chem Phys 10:6515–6526. doi:10.5194/acp-10-6515-2010
3. Bovensmann H, Burrows JP, Buchwitz M, Frerick J, Noël S, Rozanov VV, Chance KV, Goede APH (1999) SCIAMACHY: mission objectives and measurement modes. J Atmos Sci 56:127–150
4. Bracher A, Vountas M, Dinter T, Burrows JP, Röttgers R, Peeken I (2009) Quantitative observation of cyanobacteria and diatoms from space using PhytoDOAS on SCIAMACHY data. Biogeosciences 6:751–764. doi:10.5194/bg-6-751-2009
5. Burrows JP, Hölzle E, Goede APH, Visser H, Fricke W (1995) SCIAMACHY—scanning imaging absorption spectrometer for atmospheric chartography. Acta Astronaut 35:445–451
6. Carpenter LJ (2003) Iodine in the marine boundary layer. Chem Rev 103:4953–4962

7. Carpenter LJ, MacDonald SM, Shaw MD, Kumar R, Saunders RW, Parthipan R, Wilson J, Plane JMC (2013) Atmospheric iodine levels influenced by sea surface emissions of inorganic iodine. Nat Geosci 6:108–111. doi:10.1038/ngeo1687

8. Dix B, Baidar S, Bresch JF, Hall SR, Schmidt KS, Wang S, Volkamer R (2013) Detection of iodine monoxide in the tropical free troposphere. PNAS 110(6):2035–2040

9. Giese B, Laturnus F, Adams FC, Wiencke C (1999) Release of volatile iodinated C1–C4 hydrocarbons by marine macroalgae from various climate zones. Environ Sci Technol 33:2432–2439

10. Gómez Martín JC, Spietz P, Burrows JP (2007) Kinetic and mechanistic studies of the I_2/O_3 photochemistry. J Phys Chem A 111:306. doi:10.1021/jp061186c

11. Gottwald M, Bovensmann, H, Lichtenberg G, Noël S, von Bargen A, Slijkhuis S, Piters A, Hoogeveen R, von Savigny C, Buchwitz M, Kokhanovsky A, Richter A, Rozanov A, Holzer-Popp T, Bramstedt K, Lambert J-C, Skupin J, Wittrock F, Schrijver H, Burrows JP (eds) (2006) SCIAMACHY—monitoring the changing Earth's atmosphere, DLR, Institut für Methodik der Fernerkundung (IMF). Available online at http://atmos.caf.dlr.de/projects/scops/sciamachybook/sciamachybookdlr.html. Last access on 20 July 2012

12. Gottwald M, Bovensmann H (eds) (2011) SCIAMACHY—exploring the changing Earth's atmosphere. Springer, Heidelberg. doi:10.1007/978-90-481-9896-2. ISBN 978-90-481-9895-5

13. Kaleschke L, Lüpkes C, Vihma T, Haarpaintner J, Bochert A, Hartmann J, Heygster G (2001) SSM/I sea ice remote sensing for mesoscale ocean-atmosphere interaction analysis. Can J Remote Sens 27:526–537

14. Mahajan AS, Gómez Martín JC, Hay TD, Royer SJ, Yvon-Lewis S, Liu Y, Hu L, Prados-Roman C, Ordóñez C, Plane JMC, Saiz-Lopez A (2012) Latitudinal distribution of reactive iodine in the Eastern Pacific and its link to open ocean sources. Atmos Chem Phys 12:11609–11617. doi:10.5194/acp-12-11609-2012

15. Pedersén M, Collén J, Abrahamsson K, Ekdahl A (1996) Production of halocarbons by seaweeds: an oxidative stress reaction? Sci Marina 60:257–263

16. Platt U, Perner D (1980) Direct measurements of atmospheric CH_2O, HNO_2, O_3, NO_2, SO_2 by differential optical absorption in the near UV. J Geophys Res 85(C12):7453–7458

17. Platt U, Stutz J (2008) Differential optical absorption spectroscopy—principles and applications, Springer, Berlin. ISBN 978-3-540-21193-8

18. Puentedura O, Gil M, Saiz-Lopez A, Hay T, Navarro-Comas M, Gómez-Pelaez A, Cuevas E, Iglesias J, Gomez L (2012) Iodine monoxide in the north subtropical free troposphere. Atmos Chem Phys 12:4909–4921. doi:10.5194/acp-12-4909-2012

19. Richter A, Wittrock F, Eisinger M, Burrows JP (1998) GOME observations of tropospheric BrO in Northern Hemispheric spring and summer 1997. Geophys Res Lett 25:2683–2686

20. Rozanov VV, Rozanov AV, Kokhanovsky AA, Burrows JP (2014) Radiative transfer through terrestrial atmosphere and ocean: software package SCIATRAN. J Quant Spectrosc Radiat Transfer 133:13–71

21. Saiz-Lopez A, Mahajan AS, Salmon RA, Bauguitte SJ-B, Jones AE, Roscoe HK, Plane JMC (2007) Boundary layer halogens in coastal Antarctica. Science 317:348–351. doi:10.1126/science.1141408

22. Saiz-Lopez A, Plane JMC, Baker AR, Carpenter LJ, von Glasow R, Gómez Martín JC, McFiggans G, Saunders RW (2012) Atmospheric chemistry of iodine. Chem Rev 112:1773–1804. doi:10.1021/cr200029u

23. Schönhardt A, Begoin M, Richter A, Wittrock F, Kaleschke L (2012) Gómez Martín, J. C., and Burrows, J. P.: Simultaneous satellite observations of IO and BrO over Antarctica. Atmos Chem Phys 12:6565–6580. doi:10.5194/acp-12-6565-2012

24. Schönhardt A, Richter A, Wittrock F, Kirk H, Oetjen H, Roscoe HK, Burrows JP (2008) Observations of iodine monoxide columns from satellite. Atmos Chem Phys 8:637–653. doi:10.5194/acp-8-637-2008

25. Simpson WR, von Glasow R, Riedel K, Anderson P, Ariya P, Bottenheim J, Burrows J, Carpenter LJ, Frieß U, Goodsite ME, Heard D, Hutterli M, Jacobi H-W, Kaleschke L, Neff B, Plane J, Platt U, Richter A, Roscoe H, Sander R, Shepson P, Sodeau J, Steffen A, Wagner T,

Wolff E (2007) Halogens and their role in polar boundary-layer ozone depletion. Atmos Chem Phys 7:4375–4418. doi:10.5194/acp-7-4375-2007

26. Spreen G, Kaleschke L, Heygster G (2008) Sea ice remotesensing using AMSR-E 89 GHz channels. J Geophys Res 113:C02S03. doi:10.1029/2005JC00338
27. Theys N, Van Roozendael M, Hendrick F, Yang X, De Smedt I, Richter A, Begoin M, Errera Q, Johnston PV, Kreher K, De Mazière M (2011) Global observations of tropospheric BrO columns using GOME-2 satellite data. Atmos Chem Phys 11:1791–1811. doi:10.5194/acp-11-1791-2011
28. Tokarczyk R, Moore RM (1994) Production of volatile organohalogens by phytoplankton cultures. Geophys Res Lett 21(4):285–288
29. Volkamer R, Coburn S, Dix B, Sinreich R (2010) The eastern Pacific Ocean is a source for short lived trace gases: glyoxal and iodine oxide. Clivar Exchanges 53(2):30–33
30. Wagner T, Platt U (1998) Satellite mapping of enhanced BrO concentration in the troposphere. Nature 395:486–490